Analysis of Spatial Variability in Hyperspectral Imagery of the Uterine Cervix In Vivo

Michael J. DeWeert [a], Jody Oyama [a], Elisabeth McLaughlin [a], Ellen Jacobson [a], Johan Håkansson [a], Gary S. Bignami [a], Ulf Gustafsson [a], and Paul Troy [a]

Violeta Poskiene [b], Kristina Kriukelyte [b], Reda Ziobakiene [b], Aurelija Vaitkuviene [b]

Sara Pålsson [c,f], Marcelo Soto Thompson [c,f], Unne Stenram [d,f], Stefan Andersson-Engels [c,f], Sune Svanberg [c,f], Katarina Svanberg [e,f]

[a] Science and Technology International®
733 Bishop Street, Suite 3100, Honolulu, HI 96813, USA

[b] Department of Obstetrics and Gynecology
Vilnius University Hospital, Antakalnio str. 57, 2040-LT, Vilnius, Lithuania

[c] Department of Physics
Lund Institute of Technology, , P.O. Box 118, SE-221 00 Lund, Sweden

[d] Department of Pathology,
Lund University Hospital, SE-221 85 Lund, Sweden

[e] Department of Oncology
Lund University Hospital, SE-221 85 Lund, Sweden

[f] Lund University Medical Laser Centre
P.O. 118, SE-22100 Lund, Sweden

ABSTRACT

The use of fluorescence and reflectance spectroscopy in the analysis of cervical histopathology is a growing field of research. The majority of this research is performed with point-like probes. Typically, clinicians select probe sites visually, collecting a handful of spectral samples. An exception to this methodology is the Hyperspectral Diagnostic Imaging (HSDI®) instrument developed by Science and Technology International. This non-invasive device collects contiguous hyperspectral images across the entire cervical portio. The high spatial and spectral resolution of the HSDI instruments make them uniquely well suited for addressing the issues of coupled spatial and spectral variability of tissues *in vivo*. Analysis of HSDI data indicates that tissue spectra vary from point to point, even within histopathologically homogeneous regions. This spectral variability exhibits both random and patterned components, implying that point monitoring may be susceptible to significant sources of noise and clutter inherent in the tissue. We have analyzed HSDI images from clinical CIN (cervical intraepithelial neoplasia) patients to quantify the spatial variability of fluorescence and reflectance spectra. This analysis shows the spatial structure of images to be fractal in nature, in both intensity and spectrum. These fractal tissue textures will limit the performance of any point-monitoring technology.

Keywords: Cervical, Cancer, CIN, Fractal, Tissue Classification, Fluorescence, Spectroscopy, HSDI, Medical Imaging, Histopathology

1 INTRODUCTION

The use of fluorescence spectroscopy to detect pathologies in human tissue has been a field of extensive research.[1,2] Most of the research to date has involved the use of point-like probes with footprints of several hundred microns. The question of the suitability of various probe sizes has not, until now, been addressed in the literature. Further, point-monitor data are sometimes difficult to correlate with histopathology because of the uncertainties in choosing biopsy sites and the difficulties of post-biopsy registration of tissue samples.

To address the issues associated with tissue sampling and registration, we have embarked on a series of clinical studies which address the detailed spatial and spectral structure of cervical fluorescence. Spatial variability is addressed on two fronts in these studies: macroscopic and microscopic. Macroscopic structure, on the scale of 200 microns and up, is measured with HyperSpectral Diagnostic Imaging (HSDI®) devices. Case-study results of this analysis are the subject of this paper. Microscopic structure is probed via detailed histopathology studies[3] using the same data set. In addition, detailed spectral analyses of the HSDI data are correlated with detailed histopathology, and compared to point-monitor spectra.[4] This study included an unprecedented combination of detailed histopathology with high-resolution spectroscopic imaging.

In the following sections, a macroscopic analysis of the structure of HSDI images is presented. Section 2, "Materials and Methods" briefly describes the HSDI instrument and its use in a clinical study conducted in Vilnius, Lithuania. It also describes the ground-truthing of histology in the HSDI images, and the image-analysis methods. In section 3, Results, the fractal nature of fluorescence and reflectance HSDI images is presented for several imaging modes. The implications of these results for tissue probe sizes are discussed in section 4.

2 MATERIALS AND METHODS

2.1. Instrumentation

A Generation II HSDI cervical device was employed in this study. The version of the HSDI instrument used has a spatial resolution of 230 microns at its normal working distance of 0.3 meters. Images were collected in both white light reflectance and fluorescence over 50 bands spanning the spectrum from 400 nm to 760 nm. In these studies, fluorescence was excited with radiation in a band centered on 365 nm. This instrument is a refinement of the version described previously.[5]

The HSDI instruments include a high-resolution digital RGB camera, which was used to collect standard colposcopic images concurrently with hyperspectral imaging. The RGB images were used as references for registering reflectance and fluorescence.

Each subject was also examined with a point-fluorescence monitor, with an excitation peak near 337 nm. This device has been described in detail separately.[6] The point-monitor results were correlated with histpathology,[3] using the HSDI images as a guide.

2.2. Clinical

A clinical study was conducted in Vilnius, Lithuania in August and September 2001. The objective of the study was to continue the development of fluorescence hyperspectral diagnostic imaging and point monitoring techniques for the detection and localization of cervical dysplasia. The study protocol was reviewed and approved by the Institutional Review Board of Lund University Hospital and Vilnius University Hospital. The study population was a cross-section of postmenarchal women with indications for colposcopy. Subjects were recruited to undergo reflectance and fluorescence imaging and point-monitoring tissue spectrometry during their colposcopic exam. One hundred and eleven subjects were enrolled in the study. Inclusion and exclusion criteria are summarized in **Table 1**.

After obtaining informed consent, each patient's demographic data and pertinent medical histories were gathered. The patients were placed in the examination position and a vaginal speculum was inserted. The HSDI instrument was positioned to optimize the instrument's focus on the cervix. White light reflectance and UV-induced fluorescence scans (UV scans) were taken, requiring approximately 10 and 12 seconds, respectively. Following the two scans, the cervix

was cleansed with a large cotton swab soaked with a diluted acetic acid solution (3-5%) as is standard practice in colposcopic examinations. This was followed by a "post-acetic acid" white light and fluorescence scan. Both the white light scan and the UV scan are non-contact and non-invasive procedures. A standard colposcopic examination was then conducted in which the cervix was illuminated with white light, and inspected for lesions and suspicious areas. Next, the patient underwent fluorescence point monitoring. Unlike the white light and UV scans, the point monitoring does make limited contact with the surface of the cervix. Up to 36 point monitoring measurements were acquired for each patient. Based on the colposcopic examination, biopsies and miniconizations were performed after the point monitoring was completed, when applicable. The tissue samples were embedded in paraffin and processed for pathologic examination. Two independent pathologists reviewed the tissue samples. The first pathology review was conducted in Vilnius, and was used as the basis for any follow-up and treatment. One of us, Dr. Unne Stenram, conducted a second pathology review at the Lund University hospital. The second review established the ground truth for the purposes of this study.

Table 1. Criteria for Vilnius Trial Subjects

Inclusion Criteria	**Exclusion Criteria**
Age = 18	Age < 18
Indication for colposcopy or due for routine pelvic examination	Known or suspected pregnancy
No history of cervical dysplasia	
No acute diagnosis of infectious cervicovaginitis	

2.3. Post-Collection Ground-Truthing

A key part of the analysis was identification, localization and segmentation of histopathology types in the HSDI images. This segmentation served as a preliminary step prior to further image analysis. The hyperspectral images were calibrated to radiometric units, then processed to identify scan artifacts, glints and anomalous fluorescence hot spots. Each set of images was assessed to identify subjects having a complete set of high quality imaging data. For the purposes of this study, a complete image set included pre-acetic acid reflectance and fluorescence hyperspectral images, post-acetic acid reflectance and fluorescence hyperspectral images, and pre- and post-acetic acid RGB images acquired with the RGB spotting camera. Of the 111 subjects enrolled in the Vilnius study, approximately 25 data sets met all of these criteria. This paper presents the analysis of a case having high-grade CIN, with analysis of the complete set of cases to follow in future publications.

For those image regions corresponding to biopsy sites, the classification was based on microscopic examination. However, the protocol did not support biopsy of tissues with normal or non-CIN clinical presentation. For tissue not biopsied, classification was based on trained clinical judgment. **Figure 1** shows an example of the segmentation effort. After the post-acetic-acid reflectance images were classified, the classifications were transferred to the fluorescence images. Because of the viewing angles, the HSDI geometry differs slightly from the spotting camera image, complicating the transfer. This parallax adds to the labor involved in ground-truthing the images, but does not prevent us from carrying out the analysis.

2.4. Image Analysis

Two versions of each HSDI image were processed for this analysis: a pan-chromatic image and a spectral-angle map. A panchromatic (*P*) image is constructed from a HSDI data cube by summing over bands, creating a single-band (grayscale) image. Mathematically, this can be expressed as:

$$P_{ij}^{f \text{ or } r} = \sum_{k} I_{ijk}^{f \text{ or } r} \qquad (1)$$

where *i* is the line index, *j* is the sample (or column) index, and *k* is the band index. Here, $I_{ijk}^{f \text{ or } r}$ designates a calibrated hyperspectral image. The superscripts *f* and *r* designate whether the image was acquired in fluorescence or reflectance mode. The advantage of creating panchromatic images is that the sum of the bands is much less noisy than any individual band. Just as a black-and-white photograph can show much more detail than a color picture of a given

scene, so a panchromatic image allows analysis of subtle textures and spatial variations that might be missed in a band-by-band analysis of a HSDI image.

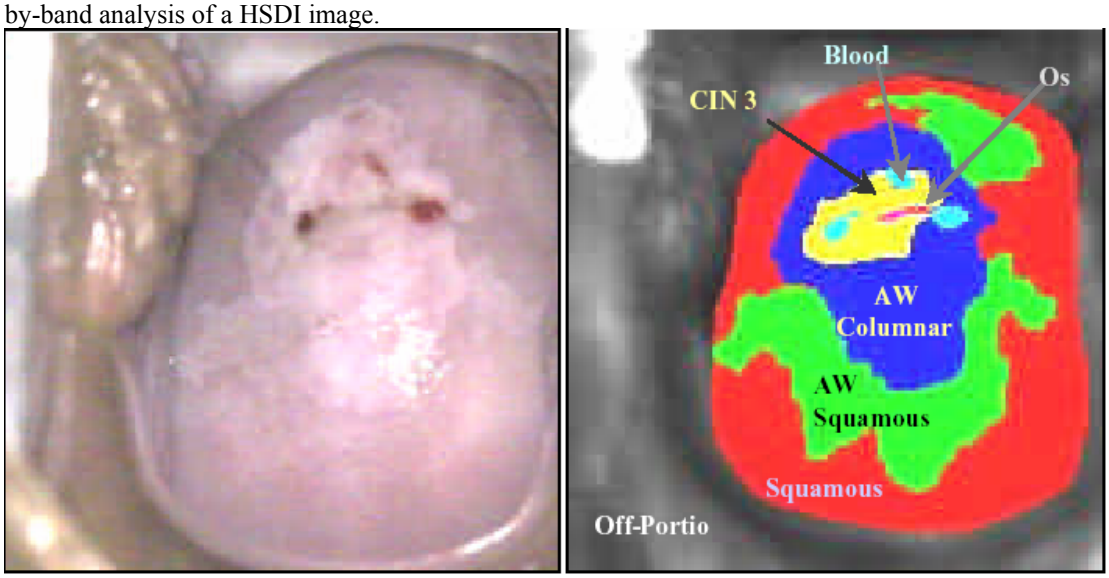

Figure 1. An example of ground-truthing the HSDI data, for subject VV0029. Left: RGB TIFF image from the spotting camera, acquired after application of acetic acid. Right: panchromatic version of a HSDI reflectance image, classified into tissue types. "AW" stands for acetowhitening.

Spectral angle maps (*SAM*s) were created by computing the angle in *N*-dimensional space (where *N* is the number of HSDI bands) between the spectrum of each image pixel and the mean spectrum of the normal (that is, non-acetowhitening) squamous tissue. For example, the SAM of a fluorescence image is:

$$SAM_{ij}^{f} = \cos^{-1}\left[\frac{\sum_{k} I_{ijk}^{f}\left\langle S_{k}^{f}\right\rangle}{\sqrt{\sum_{k}\left(I_{ijk}^{f}\right)^{2}\sum_{k}\left\langle S_{k}^{f}\right\rangle^{2}}}\right], \qquad (2)$$

where $\left\langle S_{k}^{f}\right\rangle$ is the mean spectrum of the squamous-tissue pixels. Because the image intensities are divided out in Equation (2), an SAM contains no information about the local image brightness. Rather, it contains purely spectral information. It also shares the reduced-noise property of a panchromatic image, at the expense of detailed spectral information. Since the subject of this paper is relatively subtle point-to-point spectral variability, noise suppression is critical, making this an acceptable trade-off.

Examples of panchromatic and SAM images are shown in **Figure 2**. To the human eye, these appear to have definite textures and structure, even within a single tissue type. Since these textures are subtle, compared to illumination inhomogeneity and gross inter-tissue variability, they were enhances with gradient processing. Sobel gradient filters[7] were convolved with the panchromatic and SAM images, resulting in images like those shown in **Figure 3**. This removed the gross brightness variations, making the tissue granularity more evident, both in reflectance and fluorescence images. The granularity is not just a function of brightness variations, since it shows up equally well in the purely spectral SAM images. (The reflectance images also show structure due to glints. Pixels containing these artifacts were excluded from the grain-size analysis, to avoid contaminating the results.)

The textures shown in **Figure 3** appear patterned, though not regular. That is, the images are not repetitively tiled like a honeycomb, but are also not manifestations of noise. To characterize the structure, we conducted a grain-size analysis, summarized in the flow chart shown in **Figure 4**. The grains were first counted line-by-line, then column-by-column, by comparing the gradient-filtered images to a threshold. Varying the threshold resulted in different numbers of grains, as

Figure 5 shows. The peak of the number of grains versus threshold plot is the threshold most likely to yield granularity. This peak threshold was selected for each tissue class. The frequency of grains of each size at this threshold was then computed, resulting in probability distributions like those shown in **Figure 6**.

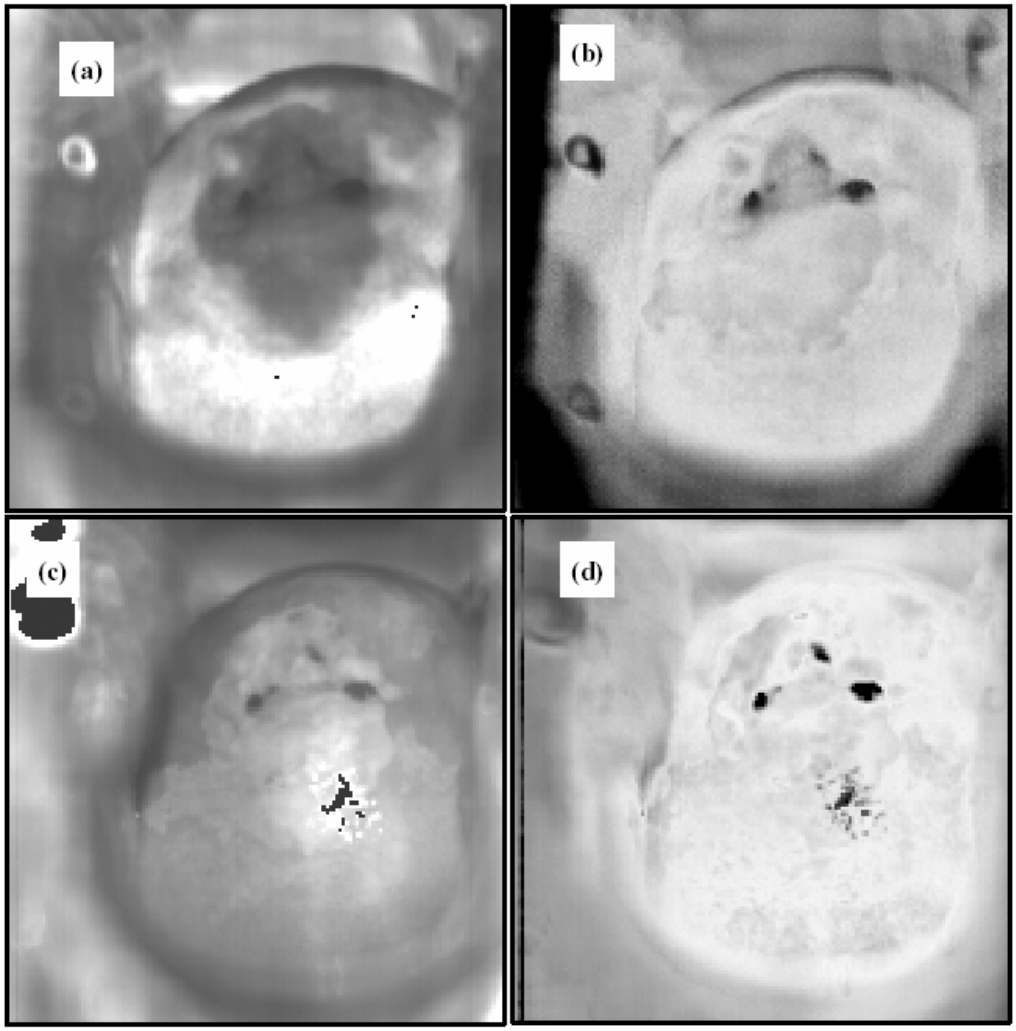

Figure 2. Panchromatic and SAM images derived from hyperspectral data, for subject VV0029, post acetic acid. (a) Panchromatic fluorescence image. (b) SAM for fluorescence, (c) Panchromatic reflectance image. (d) SAM for reflectance. The reflectance images show areas where glint was removed prior to display.

3 RESULT

Figure 6 demonstrates a classical signature of a fractal grain-size distribution: that it approximates an exponential probability distribution function (PDF):

$$PDF(x) = \frac{1}{\lambda} e^{-x/\lambda} \quad (4)$$

where λ is the characteristic decay length of the distribution. In this case, the fractal possesses not exact geometric selfsimilarity, but statistical self-similarity. The mean and standard deviation of the exponential distribution are equal:

$$\mu = \sigma = \lambda \quad (5)$$

All tissue classes in this case study are characterized by approximately exponential distributions, in both brightness and spectrum, with means and standard deviations summarized in **Figure 7**. Most tissue classes have a characteristic decay

length of 2-3 pixels, corresponding to approximately 460 – 690 microns. The non-cervical (off-portio) portion of the image has a longer characteristic length, on the order of 1150 microns.

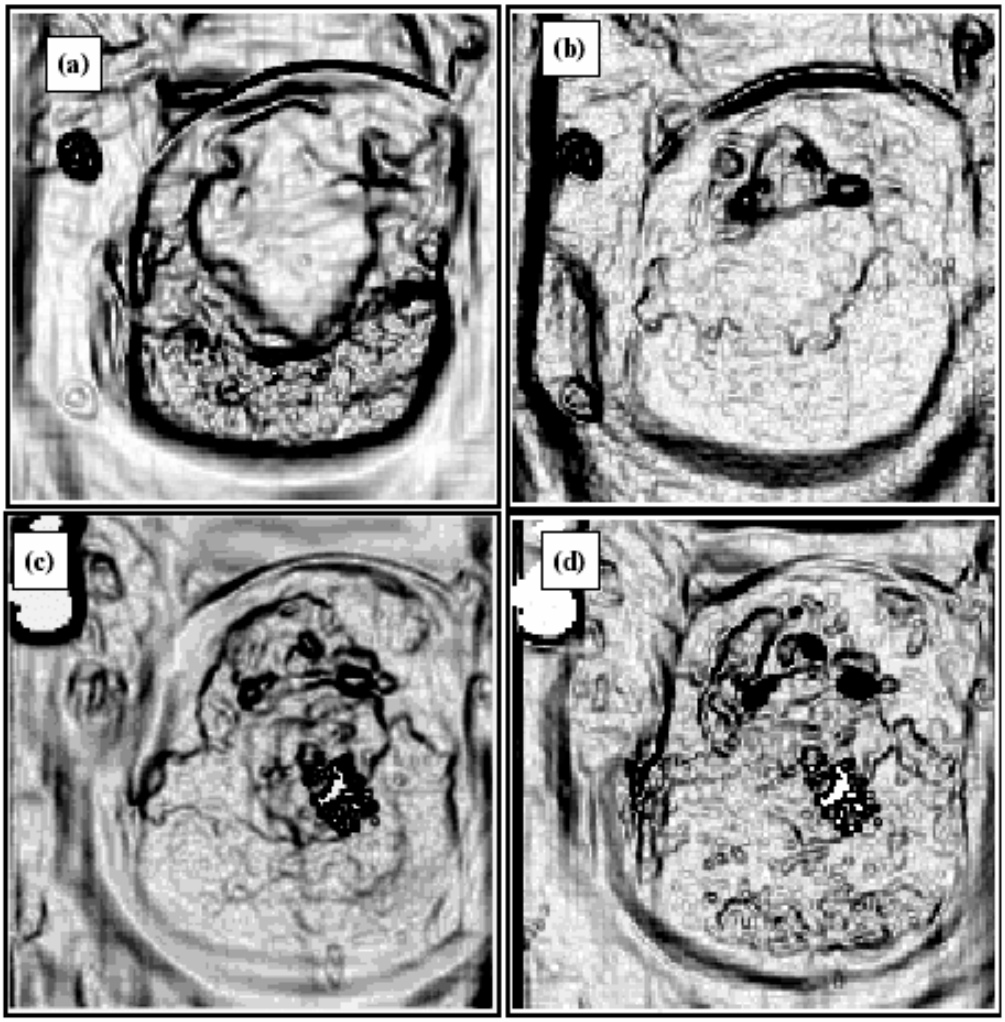

Figure 3. Gradient-processed imagery, for the cases shown in **Figure 2**. (a) Panchromatic fluorescence image. (b) SAM for fluorescence, (c) Panchromatic reflectance image. (d) SAM for reflectance.

4 DISCUSSION

The grain-size distributions shown in **Figure 6** do not show a definite peak, even at the limit of resolution of the HSDI system. This suggests that fractal structure continues to smaller grain sizes. This fractal nature is consistent with observations in the detailed histopathology studies of pathology varying from CIN to normal and back to CIN within 200 microns.[3] This is also a hallmark of fractal distributions: that the images are self-similar over length scales which vary by orders of magnitude. Of course, the upper limit of grain size is set by the physical extent of the cervical tissue.

Because the grains have a fractal distribution, there is no size of point probe which can be guaranteed to sample a "pure" spectrum in any tissue class. Nor can a large single-pixel probe size capture an "average" spectrum that can be considered truly representative of any tissue class. This variability probably contributes to the limited spectral discrimination reported for point spectroscopy in other studies.[8] Thus, spectral characterization of cervical tissues benefits from imaging spectrometers. Imaging is also required to meet the therapeutic need for tumor-margin delineation.

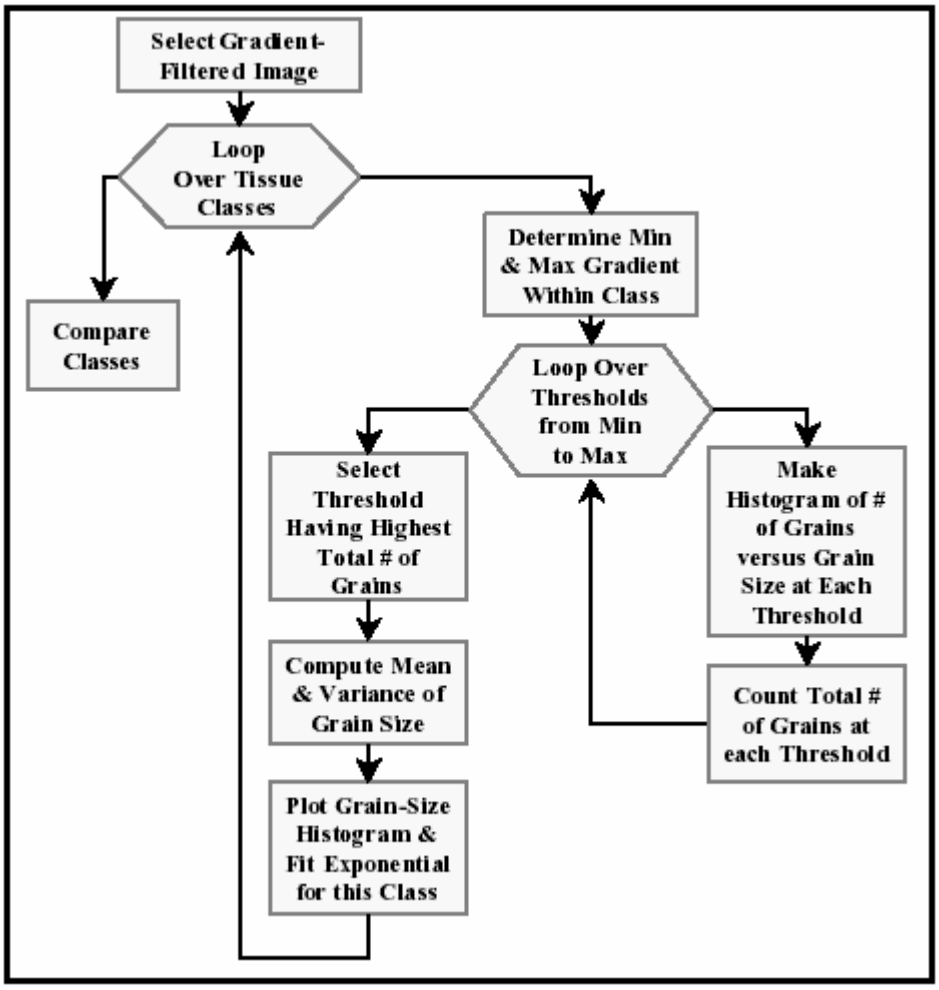

Figure 4. Flow of steps for grain-size analysis in HSDI images.

The number of contiguous pixels required to characterize a fractal surface depends on the rate at which the PDF falls with increasing grain size. However, it does *not* depend on pixel size. That is, if 1000 pixels are adequate at 200-micron resolution, 1000 pixels will be adequate at 100-micron or 300-micron resolution.

This situation is analogous to imaging, for example, the fractal pattern of an overcast sky. The image of a cloudy sky is instantly recognizable. However, the spectrum of any given pixel, taken out of context, is not cloudlike – it is just a combination of the spectra of air, water and dust. The average spectrum of a large cloud area is similarly uninformative. Overcast also has the property that its appearance is similar at ranges of 100 meters or 1000 meters, and at either range, its image is recognizably cloud-like, even though the pixel size at 1000 meters is 10 times the size at 100 meters.

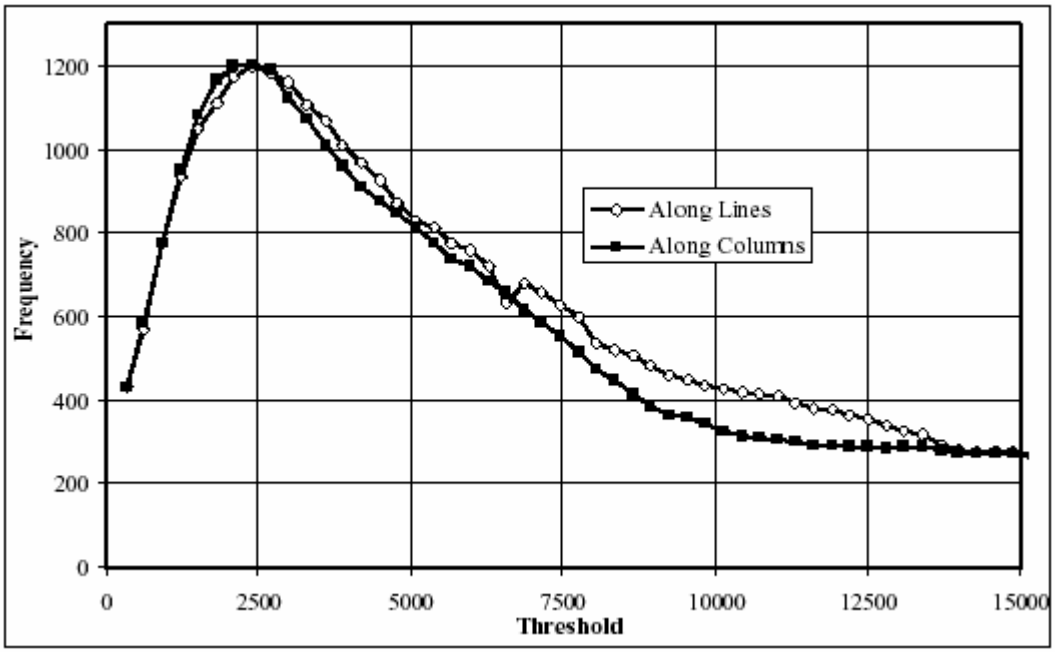

Figure 5. Number of grains versus threshold for: subject VV0029, normal squamous tissue, panchromatic fluorescence, post acetic acid. The threshold yielding the maximum number of grains was chosen for the grain-size analysis.

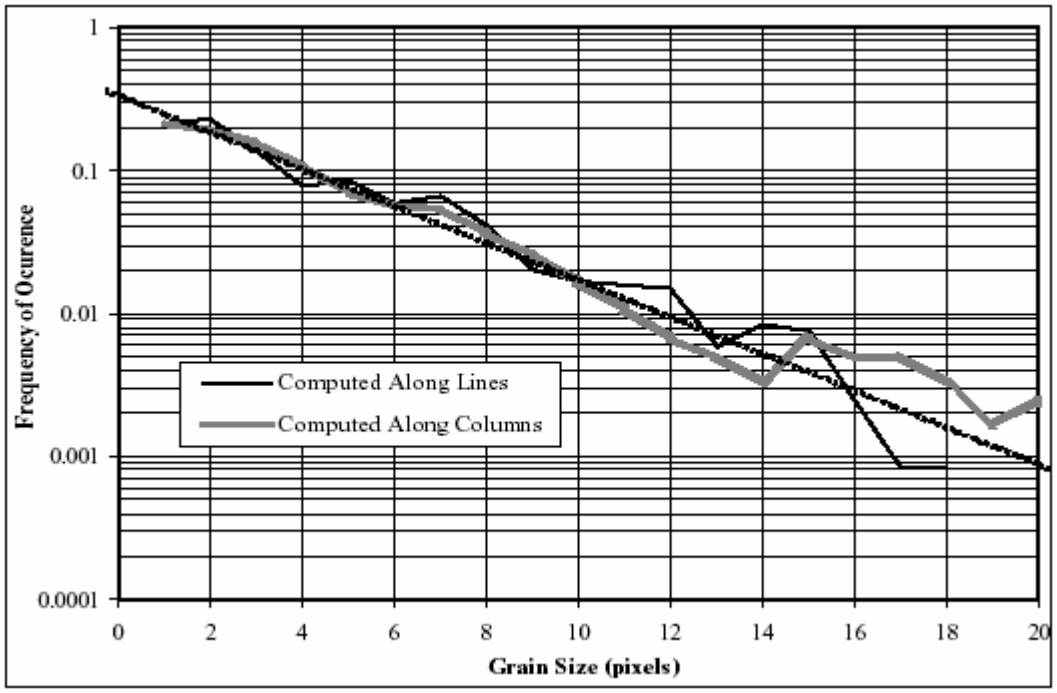

Figure 6. Number of grains versus grain size. (Computed for the gradient threshold yielding the most grains.) This approximates an exponential distribution, as indicated by the dashed trend line.

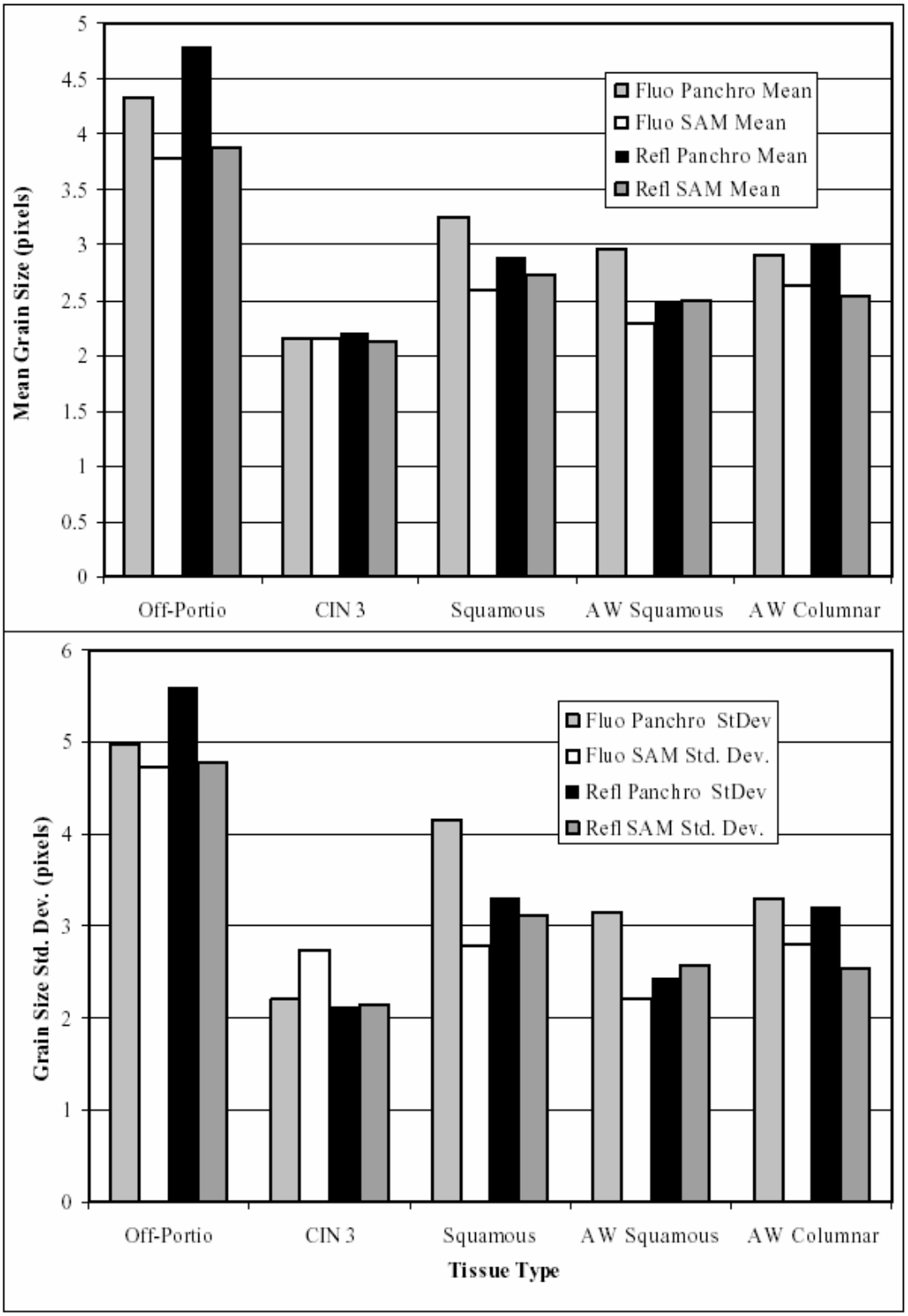

Figure 7. Mean and standard deviation of grain sizes distributions in tissue classes identified for subject VV0029.

5 CONCLUSION

This case study demonstrates that cervical tissues exhibit fractal image structure. This applies to both spectrum and intensity in fluorescence and reflectance images. This result suggests that imaging can greatly facilitate the characterization of cervical tissue. Further, the characteristic length *l* of the grain size distribution is within the Nyquist frequency of the HSDI instruments, making HSDI suitable for this analysis.

Since we have access to a uniquely large and well-characterized set of subjects, we are extending the case studies conducted so far to achieve statistically-significant measures of the fractal structure of cervical tissues. It is likely that the fractal size distribution could be a useful component of a discriminant vector for macroscopic histopathology. Medical application of these techniques could lead to a significant new technology for colposcopy. Benefits would include: reduction in the false negative rate of cervical screening, a decrease in the number and discomfort of unnecessary biopsies, and the elimination of an extended waiting period between examination and test results. Furthermore, through telemedicine, HSDI offers a means to centralize evaluation for patients in remote areas that may lack access to care or medical personnel trained to perform colposcopic examinations.

6 ACKNOWLEDGEMENT

We wish to thank the United States Army for financial support in part during the developmental phase of HSDI technology under GSA contract. We also wish to thank Dr. Jonathan Gradie of Science and Technology International for his insights and careful review of this manuscript.

7 REFERENCES

[1] See, for example: S. Svanberg, "Tissue diagnostics using lasers," in *Lasers in Medicine*, ed. R. Waynant, p. 135, CRC Press, Boca Raton (2002).
[2] See also: K. Svanberg, I. Wang, S. Colleen, I. Idvall, C. Ingvar, R. Rydell, D. Jocham, H. Diddens, S.G. Bown, G. Gregory, et al., "Clinical multi-colour fluorescence imaging of malignant tumours - Initial experience (Review)." *Acta Radiologica,* **39, issue 1**, pp. 2-9 (1998).
[3] S. Pålsson, et al. "Detailed Histopathology of Cervical Tissues In Vivo" ," Proceedings of SPIE on Spectral Imaging: Instrumentation, Applications and Analysis (BO18), BIOS 2003, SPIE, Bellingham, WA (2003).
[4] U. Gustafsson, P. Troy, M.J. DeWeert, E. Jacobson, E. McLaughlin, J. Håkansson, J. Oyama, R.B. Seiple and A. Vaitkuviene. "Fluorescence and Reflectance Imaging of Uterine Cervix In Vivo," *Proceedings of SPIE on Spectral Imaging: Instrumentation, Applications and Analysis (BO18), BIOS 2003*, SPIE, Bellingham, WA (2003).
[5] M.F. Parker, G.C. Mooradian, G.S. Okimoto, D.M. O'Connor, K. Miyazawa, S.J. Saggese, "Initial neural net construction for the detection of cervical intraepithelial neoplasia by fluorescence imaging.", Am. J. Obstet. Gynecol., **187 (2)** pp 398-402 (2002).
[6] C. Klinteberg, M. Andreasson, O. Sandstrom, S. Andersson-Engels, and S. Svanberg, "Compact fluorosensor for minimally invasive tissue characterization," Submitted for publication (2002).
[7] See, for example: A.K. Jain, *Fundamentals of Digital Signal Processing,* p. 349, Prentice Hall Inc., Englewood Cliffs, NJ (1989).
[8] N. Ramanujam, M.F. Mitchell, A. Mahadevan, S. Thomsen, A. Malpica, T. Wright, N. Atkinson and R. Richards-Kortum, "Development of A Multivariate Statistical Algorithm To Analyze Cervical Tissue Fluorescence Spectra Acquired In Vivo," *Laser Surg. Med.* **19**, 46-62 (1996).